Structure of the lunar wake: Two-dimensional global hybrid simulations

Pavel Trávníček and Petr Hellinger

Department of Space Physics, Institute of Atmospheric Physics, Academy of Sciences of the Czech Republic, Prague, Czech Republic

David Schriver

Institute of Geophysics and Planetary Physics, University of California, Los Angeles, California, USA

Stuart D. Bale

Space Sciences Laboratory and Department of Physics, University of California, Berkeley, California, USA

Received 14 December 2004; revised 8 February 2005; accepted 21 February 2005; published 22 March 2005.

[1] We study the structure and properties of the lunar wake with these solar wind parameters: the angle θ_{sw} between directions of the solar wind velocity $\boldsymbol{v}_{sw}$ and the ambient interplanetary magnetic field (IMF) $\boldsymbol{B}$ $\theta_{sw} = 45°$ and 90° and $v_{sw} = 6v_A$ (where v_A denotes solar wind Alfvén velocity). We examine the structure of the wake-tail formed behind the obstacle. In agreement with in situ observations the lunar wake is formed by two counterstreaming beams which fill the wake with a relatively cold, inhomogeneous and highly anisotropic plasma. The results of this study suggest that for given solar wind conditions the downstream region of the lunar wake is dominated by electromagnetic turbulence with the frequencies near the local proton gyrofrequency. The properties and possible generating mechanisms of the low-frequency electromagnetic turbulence are discussed. **Citation:** Trávníček, P., P. Hellinger, D. Schriver, and S. D. Bale (2005), Structure of the lunar wake: Two-dimensional global hybrid simulations, *Geophys. Res. Lett.*, *32*, L06102, doi:10.1029/2004GL022243.

1. Introduction

[2] The dominant feature of the interaction between the solar wind and the moon is the formation of a wake on the lunar nightside. The moon is essentially a non-magnetic, non-conducting obstacle which has no ionosphere. The solar wind plasma is absorbed for the most part on the dayside when it comes into contact with the lunar surface, leaving a plasma void on the nightside [*Lyon et al.*, 1967]. Since the moon acts as a diamagnetic body, the solar wind magnetic field remains unperturbed until it reaches the region on the lunar night side in the rarefied wake of a nonequilibrium plasma. As the system attempts to restore pressure balance [*Ness et al.*, 1967] the magnetic field exhibits a corresponding gradual increase. In the mid 1990's, the WIND satellite made a number of flybys of the lunar wake and the data clearly showed a number of interesting plasma physical processes. Figure 1 shows a typical example of lunar wake in situ observations by the WIND spacecraft. In particular it shows the moon wake tail encounter on Nov. 13, 1996 when the WIND spacecraft distance from the moon's center was about $25R_L$ (R_L is the lunar radius 1,738 km). The upper panel shows a gray-scale plot of the magnetic field fluctuation spectrum as a function of time and frequency. The overlaying dark curve denotes the local proton gyrofrequency. The next panel shows the gray-scale plot of the ion spectrum as a function of time and energy. The next two panels show the three components and magnitude of the magnetic field. The last panel shows the density profile. The second panel from the top of Figure 1 clearly shows counterstreaming ion beams [cf. *Ogilvie et al.*, 1996] as an important feature of the wake tail region.

[3] WIND in situ observations also show a plasma density dropout region extending to at least $7R_L$ down tail [see *Bosqued et al.*, 1996; *Owen et al.*, 1996] and various types of electrostatic and electromagnetic plasma waves, both in upwake region and in the wake-tail itself [*Kellogg et al.*, 1996; *Farrell et al.*, 1996; *Bale et al.*, 1997]. In general these observations show that kinetic processes are important in the lunar plasma environment. There are a few numerical studies of the refilling processes of the lunar wake based on full particle in cell (PIC) scheme. These include one-dimensional (1-D) self-consistent simulation studies [*Farrell et al.*, 1998; *Birch and Chapman*, 2001] using an electrostatic approximation and two-dimensional (2-D) electromagnetic simulations by [*Birch and Chapman*, 2002]. These studies focused on electrostatic, high-frequency processes.

[4] In this letter we present results of a global kinetic study of the lunar plasma environment by means of a hybrid numerical simulation with the focus being on the deep lunar wake (to tailward distances x up to $40R_L$ from the moon's center) and low-frequency electromagnetic turbulence which can occur there. We study the wake structure for these solar wind parameters: the orientation of the interplanetary magnetic field (IMF) $\theta_{sw} = 45°$ and 90°, $v_{sw} = 6v_A$, $\beta_p = 0.6$ and $\beta_e = 0.4$ (β_p and β_e being ratios between particle and magnetic pressures for protons and electrons, respectively). The lunar radius is chosen to be $R_L = 12\Lambda_i$ (Λ_i being the solar wind proton inertial length $\Lambda_i = c/\omega_{pi}$ where c is the speed of light in vacuum, ω_{pi} is the proton plasma frequency). Note that we present results (if not stated otherwise) in simulation (solar wind) units: spatial distances are given in Λ_i, time is given as the inverse of the proton cyclotron frequency Ω_i.

0094-8276/05/2004GL022243$05.00

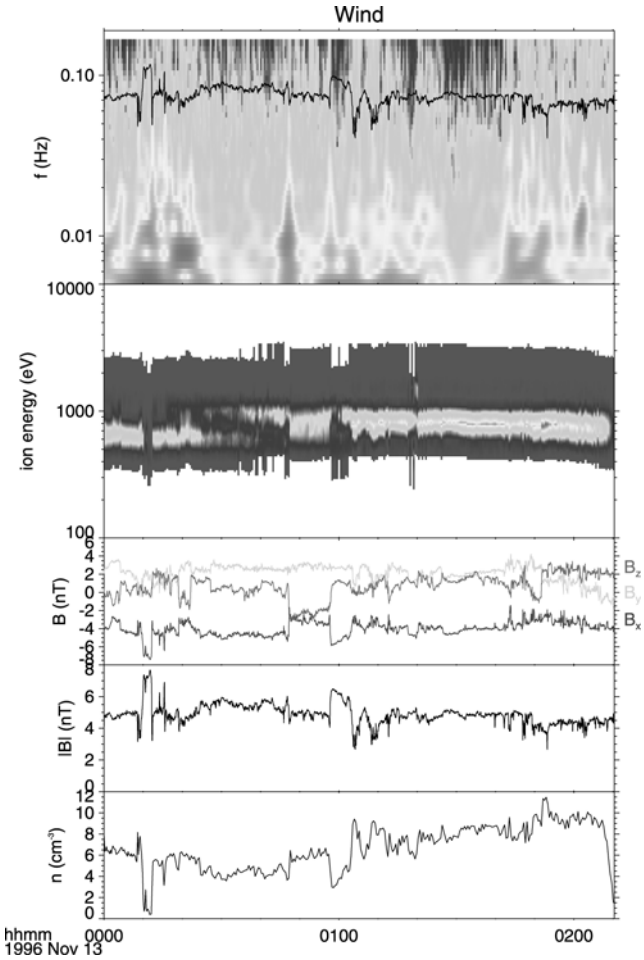

Figure 1. WIND spacecraft data from the moon wake tail encounter on 13 November 1996 (the spacecraft distance from the moon center was about $25R_L$). The upper panel shows a gray-scale plot of the wave spectra as a function of time and frequency. The overlayed curve denotes the local proton gyrofrequency. The next panel shows the gray-scale plot of the ion spectrum as a function of time and energy. The next two panels show the 3 components and magnitude of the magnetic field. The bottom panel shows the density profile. See color version of this figure in the HTML.

[5] This letter is organized as follows: First, in section 2 we describe the simulation method and then in section 3 we show results from 2.5-D global hybrid simulations (with stress on the oblique case with $\theta_{sw} = 45°$) of the lunar wake structure. Finally, in section 4 we discuss the simulation results.

2. Simulations

[6] We use a 2.5-D version of the hybrid code [*Matthews*, 1994] which has 2 spatial dimensions and 3 velocity dimensions. In this code the protons are described by a particle in cell (PIC) scheme and electrons are considered as an isothermal, isotropic, electroneutralising massless fluid. The electric field is calculated using an Ohm's law in the magnetostatic approximation and a flat resistivity term $\eta\nabla \times \boldsymbol{B}$, with $\eta = 0.02\mu_0 v_A^2/\Omega_i$ (μ_0 is the magnetic permeability of vacuum) is added to the Ohm's law. Because the electric field is proportional to the factor $1/n$ we avoid the plasma density drop out below a threshold $n_{p\min} \approx 0.01$. To do so we keep a fraction of superparticles which insulate the side of the moon facing the solar wind flow rather than remove all particles hitting the surface. We have checked that these particles does not influence our results performing several numerical experiments with different value of $n_{p\min}$ and with different number of particles per cell.

[7] We have performed two numerical experiments with different IMF orientations θ_{sw}, namely 45° and 90°. We use a selenocentric coordinate system where the x axis points tailward. IMF vectors are initialized in the 2-D simulation plane (i.e. initially $B_z = 0$). The solar wind propagates along the x axis of the simulation domain. We start the simulations with an obstacle surrounded by the homogeneous uniform flow of an isotropic Maxwellian solar wind plasma with proton and electron betas $\beta_p = 0.6$ and $\beta_e = 0.4$. The plasma is injected from the left boundary ($x \approx -5R_L$) of the simulation domain with the constant solar wind speed $v_{sw} = 6v_A$. Particles are removed at the edge of the lunar surface facing the flow to the level given by the minimum density $n_{p\min}$.

[8] We use spatial resolutions $\Delta x = 0.2\Lambda_i$ and $\Delta y = 0.25\Lambda_i$ in the x and y directions, respectively. Particles are advanced with a time step $\Delta t = 0.005\Omega_i^{-1}$. We use a substepping $\Delta t_B = \Delta t/5$ for the calculation of electromagnetic fields. We use $N_x = 3200$ and $N_y = 1280$ mesh points along the x and y directions, respectively, thus the total sizes of the simulation box are $L_x = 53R_L$ and $L_y = 26R_L$.

3. Results

[9] The equilibrium of the homogeneous solar wind is violated once the incident plasma is removed from the flow by the obstacle and a plasma void is generated. The process of the void (wake) refilling can be described by means of a plasma to vacuum expansion model and is most transparent in the solar wind rest frame. The vacuum cavity is formed behind the obstacle. The drop of the electronic pressure ($p_e = nk_BT_e \rightarrow 0$) over the distance $r_{ge} \approx 0.45$ at both edges of the cavity provides a wakeward electric force which in simulation units can be approximated by the momentum conservation law

$$\frac{dv_{py}}{dt} = \frac{e}{m_p}E_y = -\frac{\nabla p_e}{m_p n} \sim \sqrt{2\beta_{esw}}\frac{k_B v_A^2}{e\Lambda_i} = 0.89\frac{k_B v_A^2}{e\Lambda_i}, \quad (1)$$

accelerating protons in a thin layer at both edges of the cavity towards the wake center. Once the counterstreaming plasma beams are formed they begin the refilling process of the lunar cavity. The current associated with the wakeward plasma to vacuum expansion naturally leads to the gradual enhancement of the magnetic field in the lunar wake. The simulation results show that the typical wake like structure of the electric and magnetic fields known from flyby observations are formed within a tailward distance $x < 2R_L$ above the lunar surface.

[10] The enhanced magnetic field cools down the accelerated streaming plasma (see left panels of the Figure 3, cf. [*Birch and Chapman*, 2001], [*Clack et al.*, 2004]). Owing to the thermal spread v_{th} the plasma is subject to velocity filtering as the distance between warmer (faster) and colder particles increases with the distance the solar wind has

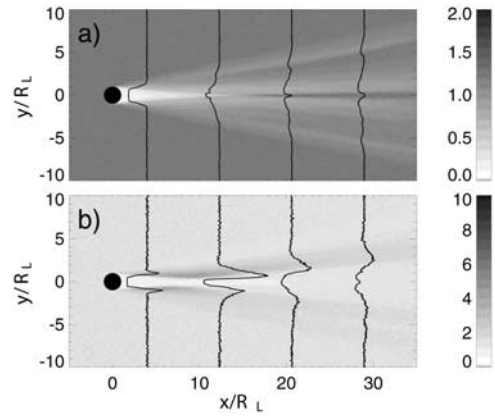

Figure 2. Gray scale plots of (a) the proton density and (b) the proton temperature anisotropy $T_{p\perp}/T_{p\|}$ are shown for the $\theta_{sw} = 45°$ simulation run. Right panels show the corresponding gray scales. Overlayed curves denote several profiles of the corresponding quantities (in arbitrary units).

convected downtail. The effective bulk velocity linearly increases at the given cut $x = x_0$ towards the wake center according to the formula [*Ogilvie et al.*, 1996]

$$v_{py'} = v_{sw} y'/x_0 + v_{th}, \quad (2)$$

where y' is distance measured towards the center of the wake from its edge ($y' = 0$). Further downtail ($x > 15R_L$) the accelerated particles build up an enhancement of the density in the wake center (see Figure 2a). The overall shape of ion reduced distribution functions (see Figure 3) qualitatively compares well with previous results of *Birch and Chapman* [2001].

[11] As the plasma is convected downtail the wakeward beams fill the lunar tail with cold plasma. The rate of the wake refilling depends on the orientation of the IMF (see Figure 4). As the angle θ_{sw} of the IMF with respect to the direction of the solar wind flow decreases the rarefied plasma tail extends to larger distances behind the moon since particles propagating along magnetic field lines have further to travel to reach the center of the plasma cavity.

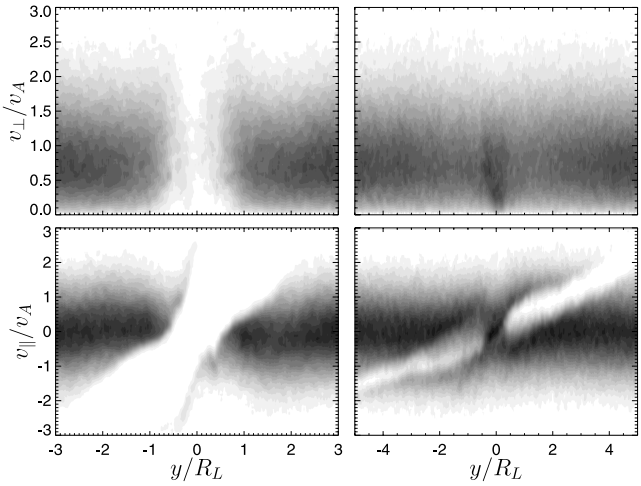

Figure 3. Reduced distribution functions (top) $f(y, v_\perp)$ and (bottom) $f(y, v_\|)$ in two regions: (left) $11.6R_L < x < 12.1R_L$ and (right) $35.6R_L < x < 37.1R_L$ (see Figure 2).

[12] The magnetic field fluctuations $|\delta\boldsymbol{B}|$ are shown in Figure 4 for both cases of $\theta_{sw} = 45°$ and $\theta_{sw} = 90°$. Note that the latter case corresponds to the 1-D PIC numerical studies performed by *Farrell et al.* [1998] and *Birch and Chapman* [2001]. The overall structure of the lunar wake is similar in both cases with $\theta_{sw} = 45°$ and $\theta_{sw} = 90°$, however, the amplitude of the magnetic field fluctuations is much higher in the first example with $\theta_{sw} = 45°$. We observe enhancements of the magnetic field magnitude associated with the rarefied plasma regions at both edges of the lunar wake. We also observe an enhancement of the magnetic field magnitude in the lunar wake center in the region $x = 0$ to $15R_L$, which is filled with rarefied plasma, whereas the amplitude of the magnetic field magnitude decreases in the wake center with enhanced plasma density further downtail ($x > 15R_L$) (see Figure 2a).

[13] Furthermore we observe low-frequency electromagnetic waves in the region $28R_L < x < 40R_L$ of the lunar wake (see Figures 4a and 5). The plasma streaming towards the wake center from both edges of the cavity builds up a region of highly anisotropic plasma (see Figure 2) and this region is subject to low-frequency turbulence. The low-frequency waves have a wave vector $k \approx 0.7$ and frequency $\omega \approx 1.2\Omega'_i$ (Ω'_i being the local gyrofrequency). These waves are present in two regions ($y < 0$ and $y > 0$) and in both regions propagate in the direction antiparallel with respect to the ambient magnetic field. These waves are left-handed in the plasma rest frame.

4. Conclusions

[14] We present results from two global simulations of the lunar wake by means of a model based on a kinetic (hybrid) scheme. The overall structure of the lunar wake as seen in these numerical experiments is in agreement with theoretical models [cf. *Whang*, 1969] and provides a global view to the in situ observations (see Figure 1). Upon contact with the surface the obstacle removes incident plasma from the solar wind and a cavity is formed. The refilling process of the cavity can be described by a plasma to vacuum expansion model. The gradient of the electron pressure leads to an electric force that accelerates plasma into the

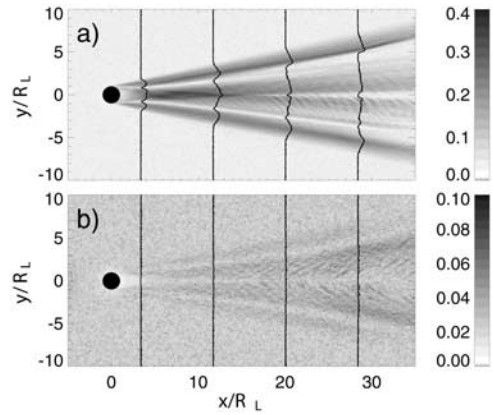

Figure 4. Gray scale plots of the magnetic fluctuations $|\delta\boldsymbol{B}|$ as a function of x and y for (a) $\theta_{sw} = 45°$ and (b) $\theta_{sw} = 90°$. Right panels show the corresponding gray scales. Overlayed curves show several corresponding profiles of $|\delta\boldsymbol{B}|$ in arbitrary units.

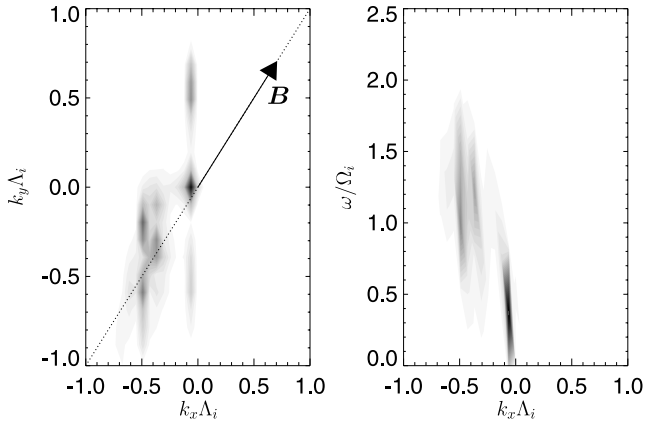

Figure 5. Gray scale plots show the Fourier analysis of the magnetic fluctuations $\delta\boldsymbol{B}$ in the simulation with $\theta_{sw} = 45°$ in the tail region $28R_L < x < 40R_L$ and $-4.4R_L < y < 4.4R_L$ (see Figure 4a) analyzed over the simulation time interval $90\Omega_i^{-1} < t < 110\Omega_i^{-1}$. The left panel shows the fluctuations $|\delta\boldsymbol{B}|$ as a function of k_x and k_y (averaged over all frequencies ω). The arrow and the dotted line indicate the background average magnetic field. The right panel shows the fluctuations $|\delta\boldsymbol{B}|$ as a function of k_x and ω (averaged over all k_y). The frequency is given in the plasma rest frame.

wake at both edges of the cavity. As the plasma moves into the cavity, two rarefaction waves propagate away from the wake's center forming edges of the lunar tail structure. The streaming plasma is subject to velocity filtering as hotter plasma moves faster into the cavity than colder plasma. The current associated with this plasma expansion is responsible for the enhancement of the magnetic field in the cavity of rarefied plasma. The enhanced magnetic field cools down the streaming plasma (see Figures 3 and 2a). The plasma convects further downtail and a region of enhanced density is formed in the wake's center where the magnitude of the magnetic field decreases (see Figures 4 and 2a).

[15] The results of our study for $\theta_{sw} = 90°$ are in qualitative agreement with earlier 1-D full particle-in-cell studies by *Farrell et al.* [1996] and *Birch and Chapman* [2001]. However we should note that the IMF orientation $\theta_{sw} = 90°$ is rare and that the case with a more realistic angle $\theta_{sw} = 45°$ is qualitatively different (see Figure 4) illustrating that the rate of the wake refilling depends on the orientation of IMF (see Figure 4).

[16] One should keep in mind that in the real (three-dimensional) lunar wake the magnetic field is also compressed in the direction perpendicular to the simulation plane. [*Owen et al.*, 1996] has discussed the presence of a system of diamagnetic currents which are formed at edges of the cavity. We observe such a formation of diamagnetic currents propagating along the z axis in our simulation, however, this process is constrained in the present study by being two dimensional.

[17] Results of our study show that two beams of counter-streaming plasma fill the lunar wake with the relatively cool, inhomogeneous and highly anisotropic plasma (see Figure 2). The results suggest that for the solar wind conditions simulated here ($v_{sw} = 6v_A$, $\theta_{sw} = 45°$), the downstream region $28R_L < x < 40R_L$ of the lunar wake is dominated by low-frequency turbulence (see Figure 5). These waves with wavenumber $k \approx 0.7$ and frequency $\omega \approx 1.2\Omega'_i$ propagate in the direction antiparallel with respect to the magnetic field. One may expect that these waves are beam-generated right-handed whistler waves [*Gary*, 1991], however, our analysis shows that the polarization of these waves is left handed. These waves propagate in the same (antiparallel with respect to the magnetic field) direction in both parts ($y < 0$ and $y > 0$) of the wake despite its overall antisymmetry in y. The polarization and the same direction of propagation indicate another generating mechanism, probably related to the anisotropy and/or heat flux (see Figure 2). A detailed study of the low-frequency wake turbulence will be the subject of future work.

[18] **Acknowledgments.** The authors acknowledge the support of grants ESA PRODEX 14529 and GACR 205/05/1011 and NSF grant INT-0010111. Wind data analysis at UC Berkeley is supported by NASA grant NAG5-11804.

References

Bale, S. D., C. J. Owen, J.-L. Bougeret, K. Goetz, P. J. Kellogg, R. P. Lepping, R. Manning, and S. J. Monson (1997), Evidence of currents and unstable particle distributions in an extended region around the lunar plasma wake, *Geophys. Res. Lett.*, *24*(11), 1427–1430.

Birch, P. C., and S. C. Chapman (2001), Detailed structure and dynamics in particle-in-cell simulations of the lunar wake, *Phys. Plasmas*, *8*(10), 4551–4559.

Birch, P. C., and S. C. Chapman (2002), Two dimensional particle-in-cell simulations of the lunar wake, *Phys. Plasmas*, *9*(5), 1785–1789.

Bosqued, J. M., et al. (1996), Moon-solar wind interaction: First results from the wind/3dp experiment, *Geophys. Res. Lett.*, *23*(10), 1259–1262.

Clack, D., J. C. Kasper, A. J. Lazarus, J. T. Steinberg, and W. M. Farrell (2004), Wind observations of extreme ion temperature anisotropies in the lunar wake, *Geophys. Res. Lett.*, *31*, L06812, doi:10.1029/2003GL018298.

Farrell, W. M., R. J. Fitzenreiter, C. J. Owen, J. B. Byrnes, R. P. Lepping, K. W. Ogilvie, and F. Neubauer (1996), Upstream ULF waves and energetic electrons associated with the lunar wake: Detection of precursor activity, *Geophys. Res. Lett.*, *23*(10), 1271–1274.

Farrell, W. M., M. L. Kaiser, J. T. Steinberg, and S. D. Bale (1998), A simple simulation of a plasma void: Applications to wind observations of the lunar wake, *J. Geophys. Res.*, *103*, 23,653–23,660.

Gary, S. P. (1991), Electromagnetic ion/ion instabilities and their consequences in space plasma: A review, *Space Sci. Rev.*, *56*, 373–414.

Kellogg, P. J., K. Goetz, and S. J. Monson (1996), Observations of plasma waves during a traversal of the moon's wake, *Geophys. Res. Lett.*, *23*, 1267–1270.

Lyon, E. F., H. S. Bridge, and J. H. Binsack (1967), Explorer 35 plasma measurements in the vicinity of the moon, *J. Geophys. Res.*, *72*, 6113.

Matthews, A. (1994), Current advance method and cyclic leapfrog for 2D multispecies hybrid plasma simulations, *J. Comp. Phys.*, *112*, 102–116.

Ness, N. F., B. W. Behannon, C. S. Scearce, and S. C. Cantarano (1967), Early results from the magnetic field experiment on Lunar Explorer 35, *J. Geophys. Res.*, *72*, 5769–5778.

Ogilvie, K. W., J. T. Steinberg, R. J. Fitzenreiter, C. J. Owen, A. J. Lazarus, W. M. Farrell, and R. B. Torbert (1996), Observations of the lunar plasma wake from the WIND spacecraft on December 27, 1994, *Geophys. Res. Lett.*, *23*(10), 1255–1258.

Owen, C. J., R. P. Lepping, K. W. Ogilvie, J. A. Slavin, W. M. Farrell, and J. B. Byrnes (1996), The lunar wake at $6.8R_L$: WIND magnetic field observations, *Geophys. Res. Lett.*, *23*(10), 1263–1266.

Whang, Y. C. (1969), Field and plasma in the lunar wake, *Phys. Rev.*, *186*, 143–150.

S. D. Bale, Space Sciences Laboratory, 7 Gauss Way, Centennial Drive at Grizzly Peak Boulevard, University of California, Berkeley, Berkeley, CA 94720-7450, USA. (bale@ssl.berkeley.edu)

P. Hellinger and P. Trávníček, Department of Space Physics, Institute of Atmospheric Physics, Academy of Sciences of the Czech Republic, CZ-141 31 Prague, Czech Republic. (trav@alenka.ufa.cas.cz)

D. Schriver, Institute of Geophysics and Planetary Physics, University of California, Los Angeles, Los Angeles, CA 90095-1567, USA. (dave@igpp.ucla.edu)